First-principles study of ω-phase formation in the Ti_3Al_2V system

2007 J. Phys.: Condens. Matter 19 386221

(http://iopscience.iop.org/0953-8984/19/38/386221)

IOP PUBLISHING JOURNAL OF PHYSICS: CONDENSED MATTER

J. Phys.: Condens. Matter **19** (2007) 386221 (10pp) doi:10.1088/0953-8984/19/38/386221

First-principles study of ω-phase formation in the Ti_3Al_2V system

M Sanati[1,2], D West[1] and R C Albers[2]

[1] Physics Department, Texas Tech University, Lubbock, TX 79409, USA
[2] Theoretical Division, Los Alamos National Laboratory, Los Alamos, NM 87545, USA

Received 2 July 2007
Published 31 August 2007
Online at stacks.iop.org/JPhysCM/19/386221

Abstract

Using first-principles methods, the phase stability of the underlying body-centered-cubic (bcc) structure of Ti_3Al_2V and slightly rearranged atomic structures are investigated. The calculated ground-state energies show an instability in the ternary Ti_3Al_2V alloy with respect to the ω structure-type atomic displacement. A Mulliken population analysis shows strong bonding between the transition metals and Al. It is shown that Ti–Al is the strongest bond and that ω-type displacements increase the population overlap for this bond and reduce the energy of the system. The first-principles calculations are extended to finite temperature and various contributions to the free energy are calculated within the quasiharmonic approximation. It is shown that, at high temperatures, the bcc structure is stabilized by the contribution of the low-energy modes to lattice entropy. In agreement with experiment and in contrast to the Ti–Al–Nb system, we find that the metastable $B8_2$ structure cannot form in this alloy.

(Some figures in this article are in colour only in the electronic version)

1. Introduction

The titanium aluminides have potential for high-temperature applications. However, a major problem in their application is their low ductility at low to intermediate temperatures. Alloying with β-stabilizing elements, such as V and Nb, is a potential method to improve their ductility [1]. To retain the benefit resulting from the additional stabilizing elements, it is evident that the possible transformations of the high-temperature ordered body-centered-cubic (bcc, B2) phase must be controlled, since those alloys which are structurally stable are serious candidates for long-term applications.

An increasing amount of data is now available concerning the phase transformation in Ti–Al–V systems [2–8]. Transmission electron microscopy (TEM) studies of ordered $(Ti, Al)_{1-x}V_x$ alloys reveal several martensitic phase transformations from the high-temperature B2 phase by cooling and aging these alloys [6–8]. The transformation of the bcc structure at high temperature to the ω-phase structure at low temperature is one of the typical

martensitic phase transformations. After the alloys were quenched and aged for several hours, the observed diffuse maxima became stronger, and it was confirmed that these diffuse maxima are due to the existence of an ordered ω-phase in the B2 matrix [6–8]. The interest in the formation of the ω-phase is due to the marked effect that this phase has on the mechanical properties of the parent phase [9]. Presence of the ω-phase in the microstructure is often detrimental to the ductility.

The mechanism generally assumed for the bcc–ω transformation is the collapse of the $\{111\}_\beta$ plane due to a $2/3\langle 111\rangle_\beta$ longitudinal displacement wave [9]. Thus, when the ω-phase is created, two neighboring (111) planes move toward each other by a displacement in the [111] direction, while each third plane remains unmoved. This type of transformation is called displacive because it involves cooperative movement over small distances which are fractions of lattice translation vectors. In contrast, a diffusion-controlled nucleation and growth transformation occurs via atomic diffusion.

In the alloy with chemical composition near $Ti_3Al_{2.1}V_{0.9}$ after aging for 50 h at 793 K an ordered ω-phase has been observed [6, 7]. The ω-phase is a known precursor to the $B8_2$ phase in the Ti–Al–Nb system with comparable composition [10, 11]. The observed path, B2 $\rightarrow$ ω'' $\rightarrow$ $B8_2$, traverses a state of minimum symmetry (ω, $P\bar{3}m1$) that is a subgroup of both $Pm\bar{3}m$ and $P6_3/mmc$. This space group of minimum symmetry is the intersection of the parent and product space groups. The formation of ω as an intermediate metastable phase provides a continuous structural path for the alloy to accomplish the B2 to $B8_2$ transition. The direct B2 $\rightarrow$ $B8_2$ transformation occurs by a reconstructive transformation without the formation of the intermediate trigonal phase. Since V and Nb belong to the same group of the periodic table and have similar valence structures, it is expected that the Ti–Al–V system will also show a similar transformation. However, for the Ti–Al–V system the observed ordered ω-phase is trigonal with a space group $P\bar{3}m1$, and a transformation to the $B8_2$ phase has not been seen.

So far there has been no theoretical study of the B2, ω, and $B8_2$ phases in Ti–Al–V alloys and the number of experimental studies are also limited. Reliable information, such as crystal lattice parameters, bulk modulus, heat of formation, and phonon densities of states, is also lacking. Furthermore, there is very little understanding of the instability of the underlying bcc structure against the ω-type distortions from the electronic perspective.

In the present investigation we use first-principles methods to study the formation of the ω-phase in the Ti_3Al_2V system. The lattice parameters, bulk modulus, and heat of formation for underlying bcc and related ω-phases are calculated. We show that the instability of the underlying bcc structure against the ω-phase can be explained in terms of strong Ti–Al bonds. By calculating the Helmholtz free energy within the quasiharmonic approximation, we extend our studies to finite temperature. It is shown that excess vibrational entropy stabilizes the high-temperature underlying bcc phase. In agreement with experiment, we show that the $B8_2$-phase cannot form in this system.

2. Methodology

The present calculations were carried out using two first-principles density-functional packages, VASP [12–15] and SIESTA [16, 17], within the generalized gradient approximation to the exchange–correlation potential (see references [18] for VASP and [19] for SIESTA). We use SIESTA for the Mulliken population analysis, while VASP is used for the rest of the calculations.

The VASP calculations use plane-wave basis sets and ultrasoft Vanderbilt-type pseudopotentials [21]. In the VASP approach, the solution of the generalized self-consistent

Table 1. Calculated crystal parameters, bulk modulus (B), and heat of formation (E_{HF}) of Ti_3Al_2V BOT and ω'' structures.

	a (Å)	c (Å)	$z + 1/6$	B (GPa)	E_{HF} (eV/atom)
BOT	4.485	5.493	0.167	121.5	−0.257
ω''	4.525	5.407	0.230	117.5	−0.274

Kohn–Sham equations are calculated using efficient matrix-diagonalization routines based on a sequential band-by-band residual minimization method and Pulay-like charge density mixing [22]. We used a plane-wave basis cutoff at 304.7 eV for all structures. Electronic degrees of freedom were optimized with a conjugate gradient algorithm, and both the cell constants and ionic positions are fully relaxed. The crystal is represented by 6-atom or 12-atom periodic cells. A $7 \times 7 \times 5$ Monkhorst–Pack [20] mesh is used to sample the Brillouin zone. The dynamical matrix calculations were performed using the force-constant method in a 108-atom cell with k-point sampling of $2 \times 2 \times 2$.

The SIESTA calculations use norm-conserving pseudopotentials in the Troullier–Martins form [23] to remove the core regions from the calculations. The basis sets for the valence states are linear combinations of numerical atomic orbitals [16, 24, 25]. In the present calculations, we use double-zeta polarized basis sets (two sets of valence s and p orbitals plus one set of d orbitals). The charge density is projected on a real-space grid with an equivalent cutoff of 150 Ryd to calculate the exchange–correlation and Hartree potentials.

The eigenvalues of the dynamical matrix are the normal-mode frequencies, ω_s, of the system. The knowledge of all normal modes of the supercell also allows the construction of the phonon density $g(\omega)$. This function is obtained by evaluating the dynamical matrix at 10 000 k points in the Brillouin zone of the supercell. Once $g(\omega)$ is known, the Helmholtz vibrational free energy F_{vib} is straightforward to calculate [26, 27].

3. First-principles calculations at $T = 0$ K

To understand a crystal structure from first principles, it is first useful to determine the overall unit cell. The unit cell has six atoms for the Ti_3Al_2V system, as shown in figure 1. We constrained the c/a ratio to $\sqrt{6}/2$ (ideal value), and determined the lattice constant, a. After studying all the possible arrangements of the atoms in the six-atom unit cell, we found that the atomic configuration in figure 1(a) has the lowest energy. (For convenience, from now on, the structure shown in figure 1(a) is referred to as the body-centered-orthogonal ternary (BOT) structure.) This finding is similar to that in the Ti–Al–Nb system in which Ti atoms tend to occupy one site while Al and Nb tend to occupy the other sites of the bcc structure [28]. We varied the positions of the planes along $[111]_{bcc}$ and optimized the lattice parameters for each new configuration. The calculated total energy versus plane displacement z (where z is a dimensionless variable varying between 0 and 1/12 in terms of c/a unit) is shown in figure 2. The lattice with $z = 0$ corresponds to a bcc structure. The complete ω-phase is formed when $z = 1/12$; for the other values of z, the structures are the 'incomplete' ω-phase (ω''). Finally the structure parameters were optimized around the minima of the energy (figure 2). Calculated atomic parameters for BOT and ω'' structures are given in table 1.

To understand the origin of the instability of the BOT structure, we use a Mulliken overlap population analysis (MOPA) for studying the bonding between different elements as a function of atomic displacement z. Figure 3 demonstrates several important results. (i) The Ti–Al bonds have the highest population overlap with respect to Ti–V and V–Al bonds. (ii) Approaching

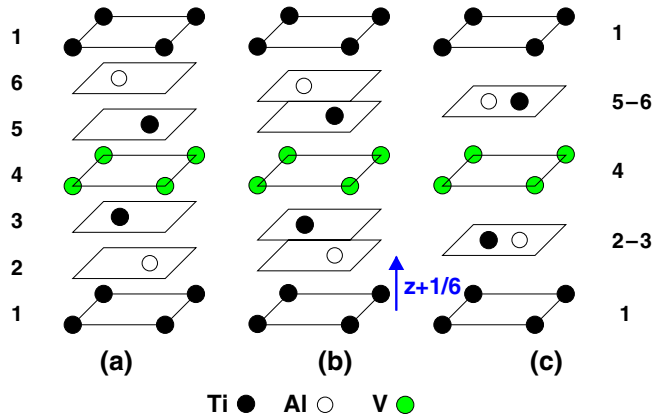

Figure 1. (a) Stacking of the (111) planes of the underlying bcc (BOT) Ti_3Al_2V structure, (b) ω''-phase (partial collapse of the planes), (c) ω structure (full collapse of the planes).

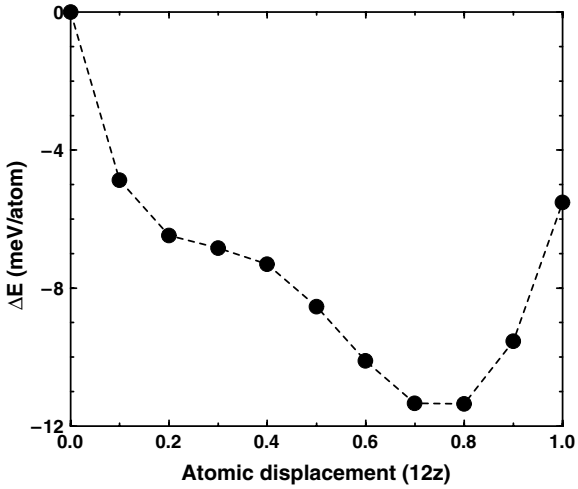

Figure 2. Calculated total energy as a function of atomic displacement for the Ti_3Al_2V system.

Ti–Al bonds have higher overlap at shorter distances (large z). (iii) Receding Ti–Al bonds show an increase in overlap at the beginning of the collapse and after that a reduction in the overlap population. This is evidence of strong directional bonding between Ti(d) and Al(p) electrons. (iv) The population overlap between receding Ti and V atoms decreases while that for approaching V and Al atoms increases. This confirms the importance of the second-nearest neighbor in this type of transformation, which has been also observed in Ni–Al system [29].

The MOPA results are also in agreement with the results of the x-ray photoelectron spectroscopy (XPS) studies of Ti–Al and Ti–Al–V alloys [30] which indicate charge transfer from the Al sites toward the transition metal sites. Therefore, the instability of the BOT structure with respect to the ω''-type displacement is a consequence of the strong bonding between the Ti d electrons and Al p electrons. The Ti–Al bond is the strongest bond among all of the present bonds. This bond is stronger at shorter distances, relative to its position in the BOT structure. Therefore, one expects to see the instability of the BOT structure with respect to the ω''-phase. In this way, the Ti–Al bond reduces its energy.

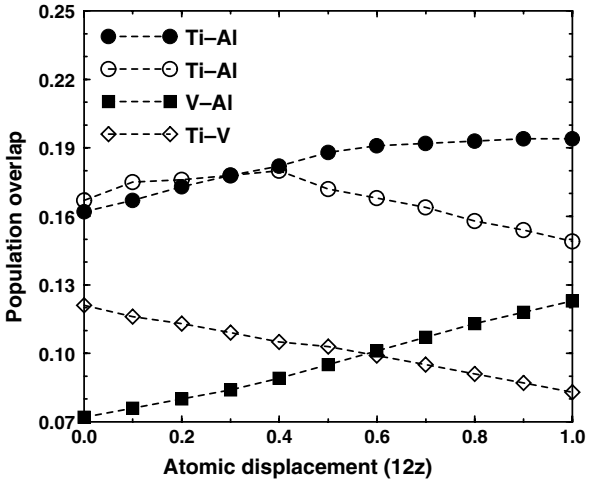

Figure 3. The population overlap for different bonds as a function of atomic displacement z. The approaching (receding) bond is shown with solid (empty) symbols, where approaching (receding) indicates decreasing (increasing) bond length with increasing z.

In order to determine heats of formation, we first calculated the total energies of elemental Ti, Al, and V corresponding to their respective equilibrium lattice parameters. Note that first-principles calculations predict the ω-phase as the true ground state of Ti rather than hexagonal close-packed (hcp) [27]. In this calculation, only the hcp structure has been used. At zero temperature, there is no electronic entropy contribution to the free energy and the vibrational zero point energy is very small compared to that of the ions.

The heat of formation per atom (E_{HF}) can be obtained from the following relation:

$$E_{\mathrm{HF}} = \tfrac{1}{6}[E_{\mathrm{Ti_3Al_2V}} - (3E_{\mathrm{Ti}} + 2E_{\mathrm{Al}} + E_{\mathrm{V}})] \tag{1}$$

where $E_{\mathrm{Ti_3Al_2V}}$ refers to the total energy of the BOT phase or the ω''-phase at equilibrium volume. The calculated values for BOT and ω'' are given in table 1.

4. Finite-temperature results

The thermodynamical quantity determining the phase stability is the Gibbs free energy $G(P, T)$, where P and T are the pressure and temperature of the system, respectively. However, for simplicity, all calculations are carried out at equilibrium volume ($P = 0$). In this case, the Gibbs free energy reduces to the Helmholtz free energy. At high temperatures, entropy effects may play an important role in determining the phase stability. There are a number of contributions to the entropy, such as electronic, vibrational, and configurational.

The electronic contribution to the free energy depends on the electronic density of states (DOS) as a function of volume, $n(E, V)$. The occupation of these states, given by the Fermi distribution $f(E, T) = [\mathrm{e}^{(E-E_{\mathrm{f}})/(K_{\mathrm{B}}T)} + 1]^{-1}$, determines their entropy [31],

$$S_{\mathrm{el}}(T, V) = -k_{\mathrm{B}} \int [f \ln f + (1 - f)\ln(1 - f)]n(E, V)\,\mathrm{d}E, \tag{2}$$

and hence the electronic contribution to the free energy $F_E(T, V) = -T S_{\mathrm{el}}(T, V)$. Although the electronic entropy terms are not large, we include them in our calculations for completeness.

The vibrational modes of the crystal are an important contribution to the free energy of the system; the magnitude of the vibrational entropy is generally larger than the electronic

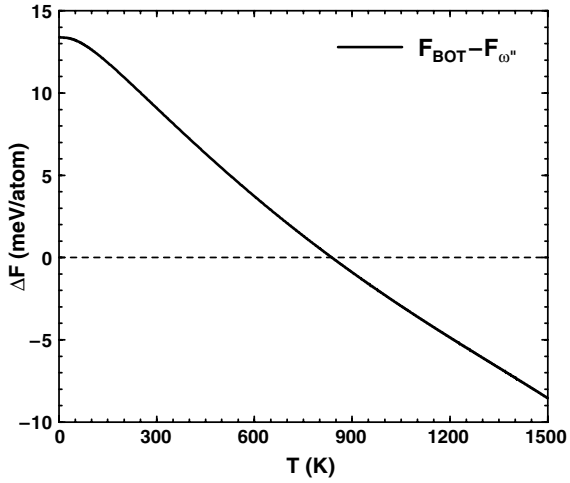

Figure 4. The total free-energy difference of the BOT phase and the ω''-phase as a function of temperature. Below 837 K the ω''-phase is more stable than the BOT phase.

one. Far from the melting point, the vibrational free energy $F_{\rm vib}$ can be calculated within the quasiharmonic approximation [15, 32]. This is similar to calculating $F_{\rm vib}$ in the harmonic approximation, retaining only the implicit volume dependence through the frequencies as [33]

$$F_{\rm vib}(T, V) = 3k_{\rm B}T \int_{\Omega} \ln\left\{2\sinh\left(\frac{\hbar\omega}{2k_{\rm B}T}\right)\right\} g(\omega, V)\, {\rm d}\omega. \tag{3}$$

The phonon densities of states are calculated at a few volumes and then interpolated to get the volume dependence. The quasiharmonic approximation accounts only partially for the effects of the anharmonicity, through the volume dependence of the phonon spectra. However, it turns out to be a very good approximation at temperatures not too close to the melting point [32].

4.1. BOT → ω″ transformation

Figure 4 shows the difference between the Helmholtz free energies of the BOT and ω'' structures. Above 837 K the BOT structure is more stable than ω''-phase. By reducing the temperature below this temperature, the metastable ω-related phase (ω'') forms. This result is in excellent agreement with the observed temperature of 793 K [6, 7]. The slight difference can be caused by the small difference between the theoretical and experimental concentrations of the alloys.

In figure 5, the phonon densities of states for the BOT phase and the ω''-phase at the predicted transition temperature are shown. The calculated phonon density of states consists of two bands separated by a gap for both structures. The Ti and V related modes are at low energies and the Al ones are at high energies (frequencies). In the BOT structure, phonons in both bands are shifted to the lower frequencies with respect to the ω''-phase. The high-frequency modes are due to the strong bonding between the transition metals (Ti and V) and Al atoms and the change of the nearest-neighbor atoms with respect to the BOT structure. We did not find any imaginary vibrational frequencies for the BOT structure. Therefore, we support the model of Friedel [34] that the excess entropy for the bcc phase is due to an overall lower phonon spectrum, expected to scale with the number of neighbors.

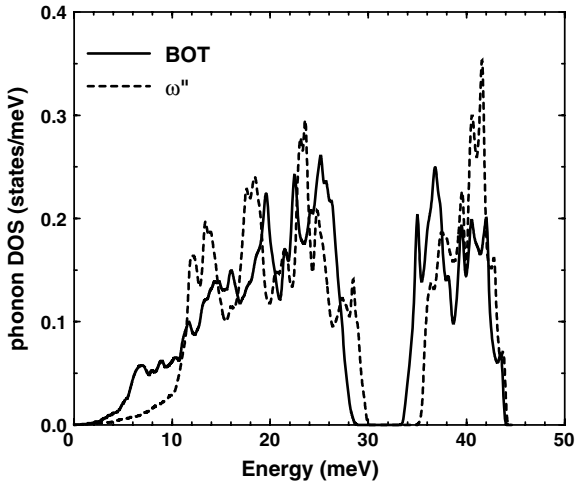

Figure 5. The phonon DOS for the B2 (solid line) and ω (dashed line) phases at $T = 837$ K.

4.2. $B8_2$ structure stability

The ω-phase is a known precursor to both the O (orthorhombic) and $B8_2$ phases in the Ti–Al–Nb system. For example, in $Ti_3Al_{2.25}Nb_{0.75}$ alloy, annealing of the ω''-phase results in the metastable $B8_2$ (isothermal ω)-phase [10, 11]. In the $B8_2$ structure, the double layers (planes 2–3 and 5–6 in figure 1(c)) are completely composed of Ti and Al, with all of the V found on the single layers [11]. In figure 1(c), one of the possible configuration of the $B8_2$ structure is shown. It has been shown that, at finite temperature, distinct configurations of the Ti_3Al_2Nb system are degenerate [28]. Furthermore, it is this configurational entropy that stabilizes the $B8_2$ structure with respect to the ω''-phase. However, such a structure for the Ti–Al–V system has not yet been observed.

In figure 1(c), the exchange of the V atoms in the fourth plane with Ti atoms in the first plane does not create a new configuration due to periodic boundary conditions and the translational symmetry of the crystal. Therefore, one needs to consider a bigger unit cell. The two lowest-energy 12-atom configurations are shown in figure 7. These distinct configurations are called $B8_2$(a) and $B8_2$(b). The ground-state energy calculations show that $B8_2$(a) has 1.2 meV/atom lower energy than $B8_2$(b). Comparison of the Helmholtz free energy of the two structures shows that the $B8_2$(a) structure is also the most stable configuration at finite temperature (figure 6). In contrast to the Ti_3Al_2Nb system, the energy of the different $B8_2$ configurations does not become degenerate at any temperature. Therefore, configurational entropy can not contribute to the total free energy of this system. The differences between the Ti–Al–Nb and Ti–Al–V systems can be explained in terms of the chemical bonding between the atoms. For the Ti_3Al_2Nb system, the $B8_2$(b) structure is more stable than $B8_2$(a) by 4 meV/atom ($T = 0$ K). The $B8_2$(b) structure has more V–V (Nb–Nb) bonds with respect to the $B8_2$(a) structure. The bcc cohesive energies [35] for V and Nb are 511 and 718 kJ mol^{-1}, respectively. Thus, V–V is a weaker bond with respect to Nb–Nb bond and this will limit the number of possible degenerate structures.

Note that our calculations also predict that the direct B2 $\rightarrow$ $B8_2$ transformation cannot happen. This is because the ω''-phase is the precursor of the $B8_2$ transformation, and our results confirm that at all temperatures the ω''-phase is more stable than $B8_2$ (figure 6).

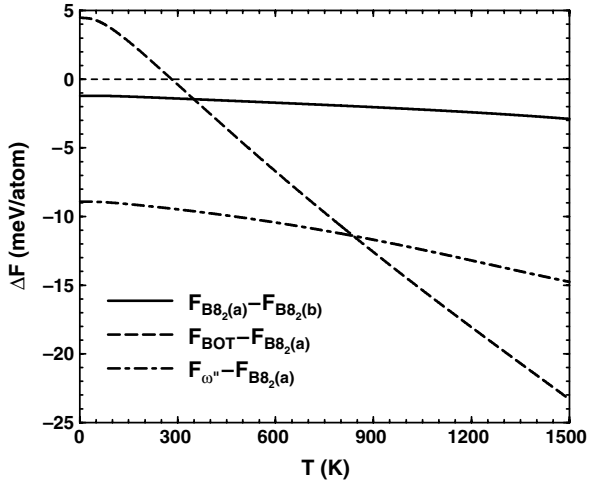

Figure 6. The total free-energy difference between $B8_2$(a) and $B8_2$(b)), BOT and $B8_2$(a), and ω'' and $B8_2$(a) structures.

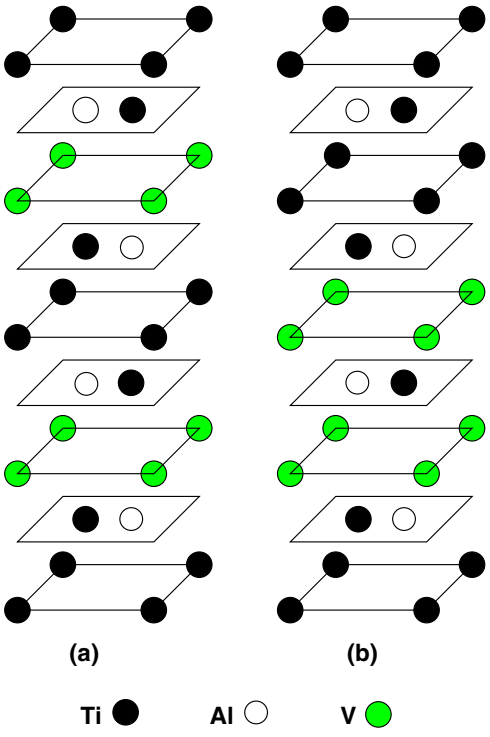

Figure 7. Different atomic configurations of the $B8_2$ structure with the two lowest ground-state energies.

5. Summary

We have performed first-principles calculations to study the stability of the underlying bcc, ω'', and $B8_2$ structures of the Ti_3Al_2V system. The lattice parameters, bulk modulus, and heat of

formation for the underlying bcc and ω''-phases have been calculated. The Mulliken population analysis shows strong bonding between the transition metals and Al. It is shown that Ti–Al is the strongest bond and ω-type displacements will increase the population overlap for this bond. This bond is stronger at shorter distances, relative to its position in the BOT structure. Therefore, the system reduces its energy by undergoing ω-type displacements.

The various contributions to the free energy of different metastable phases have been calculated. The vibrational free energy was obtained from first principles in the quasiharmonic approximation. The electronic entropy contribution to the free energy for all of the phases was calculated. We showed that the underlying bcc structure is stabilized by excess vibrational entropy against the ω'' and $B8_2$ phases. The phonon density of states for each structure at the transition temperatures was calculated. The predicted transition temperatures are in excellent agreement with available experimental results.

It is confirmed that, in contrast to the Ti–Al–Nb system, in this system the $B8_2$ structure cannot be formed. It is shown that, due to the weak V–V interaction, configurational entropy cannot play any role in this transition.

Acknowledgments

This work was carried out under the auspices of the Advanced Research Program of the State of Texas and the National Nuclear Security Administration of the US Department of Energy at Los Alamos National Laboratory under contract no. DE-AC52-06NA25396. The generous amounts of computer time provided by Texas Tech's High Performance Computer Centre was much appreciated.

References

[1] Izumi O (ed) 1991 *Proc. Int. Symp. on Intermetallic Compounds* (Sendai: JIM Publications)
[2] Raghavan V 2005 *J. Phase Equilib. Diffus.* **26** 276
[3] Tsakiropoulos P and Shao G 2004 *Mater. Sci. Eng.* A **375–377** 201
[4] Shao G and Tsakiropoulos P 2002 *Mater. Sci. Eng.* A **329–331** 914
[5] Diplas S, Tsakiropoulos P, Shao G, Watts J F, Tsakiropoulos P, Shao G and Matthew J A D 2002 *Acta Mater.* **50** 1951
[6] Shao G, Tsakiropoulos P and Miodownik A P 1996 *Mater. Sci. Eng.* A **216** 1
[7] Shao G, Miodownik A P and Tsakiropoulos P 1995 *Phil. Mag.* A **71** 1389
[8] Ahmed T and Flower H M 1992 *Mater. Sci. Eng.* A **152** 31
[9] Sikka S K, Vohra Y K and Chidambaran R 1982 *Prog. Mater. Sci.* **27** 245
[10] Sadi F A and Servant C 2000 *Phil. Mag.* A **80** 639
[11] Bendersky L A, Boettinger W J, Burton B P and Biancaniello F S 1990 *Acta Metall. Mater.* **38** 931
[12] VASP 2003 at http://cms.mpi.univie.ac.at/vasp
[13] Kresse G and Hafner J 1993 *Phys. Rev.* B **47** 558
[14] Kresse G and Furthmüller J 1996 *Phys. Rev.* B **54** 11169
[15] Kresse G and Joubert D 1999 *Phys. Rev.* B **59** 1758
[16] Sánchez-Portal D, Ordejón P, Artacho E and Soler J M 1997 *Int. J. Quantum Chem.* **65** 453
[17] Artacho E, Sánchez-Portal D, Ordejón P, García A and Soler J M 1999 *Phys. Status Solidi* b **215** 809
[18] Perdew J P 1991 *Electronic Structure of Solids '91* ed P Ziesche and H Eschring (Berlin: Akademie) p 11
[19] Perdew J P, Burke K and Ernzerhof M 1996 *Phys. Rev. Lett.* **77** 3865
[20] Monkhorst H J and Pack J D 1976 *Phys. Rev.* B **13** 5188
[21] Vanderbilt D 1990 *Phys. Rev.* B **41** 7892
[22] Kresse G and Furthmüller J 1996 *Comput. Mater. Sci.* **6** 15
[23] Troullier N and Martins J L 1991 *Phys. Rev.* B **43** 1993
[24] Sankey O F and Niklevski D J 1989 *Phys. Rev.* B **40** 3979
Sankey O F, Niklevski D J, Drabold D A and Dow J D 1990 *Phys. Rev.* B **41** 12750
[25] Demkov A A, Ortega J, Sankey O F and Grumbach M P 1995 *Phys. Rev.* B **52** 1618

[26] Estreicher S K, Sanati M, West D and Ruymgaart F 2004 *Phys. Rev.* B **70** 125209
[27] Rudin S P, Jones M D and Albers R C 2004 *Phys. Rev.* B **69** 094117
[28] Sanati M, West D and Albers R C 2007 submitted
[29] Sanati M, Albers R C and Pinski F J 2001 *J. Phys.: Condens. Matter* **13** 5387
[30] Diplas S, Watts J F, Tsakiropoulos P, Shao G, Beamson G and Matthew J A D 2001 *Surf. Interface Anal.* **31** 734
[31] Watson R E and Weinert M 2001 *Solid State Physics* vol 56, ed H Ehrenreich and F Spaepen (San Diego, CA: Academic) p 85
[32] Kern G, Kresse G and Hafner J 1999 *Phys. Rev.* B **59** 8551
[33] Baroni S, de Gironcoli S, Dal Corso A and Giannozzi P 2001 *Rev. Mod. Phys.* **73** 515
[34] Friedel J 1974 *J. Phys. Lett.* **35** L59
[35] Young D A 1991 *Phase Diagrams of the Elements* (Berkeley, CA: University of California Press)